Development of Discrete Nanopores. II. Comparison between Layered Films and Blends of Polyolefins

Jonghwi Lee, Christopher W. Macosko, Frank S. Bates

Chemical Engineering and Materials Science, University of Minnesota, Minneapolis, Minnesota 55455

Received 9 February 2004; accepted 28 June 2004
DOI 10.1002/app.21221
Published online in Wiley InterScience (www.interscience.wiley.com).

ABSTRACT: Discrete nanopores develop in the interfacial regions of polyolefin blends and layered films under tension. They originate from crazelike structures in the early development stage, which later undergo disruption processes with an increase in strain. The disruption processes appear to be triggered by the existence of adjacent ductile polyolefins and their micromechanical deformations. The degree of nanopore development significantly varies among blends and layered systems, depending on several material parameters, such as the interfacial strength. Discrete nanopores are observed more often in metallocene systems and blends than in Ziegler–Natta systems and layered films. Macroscopically, with the development of discrete nanopores, metallocene systems show higher strain to break and significant shear yielding under tension. The disruption mechanism can be used to prepare nanoporous materials or to improve the mechanical performances of polyolefins.
 J Appl Polym Sci 95: 708–718, 2005

Key words: crazing; films; polyethylene (PE); polyolefins; poly(propylene) (PP); shear; yielding

INTRODUCTION

The mechanical response of a material is an important factor in the selection of the appropriate material for a given application. The mechanical energy given to materials can be elastically stored and also irreversibly dissipated. In typical mechanical tests, the initial reversible deformation is usually distinguished by the modulus, whereas the following irreversible deformation is characterized by the yield stress or stress to break (strength).[1] Because macroscopic mechanical responses reflect the characteristics of micromechanical deformations, the initiation and growth of the deformations are critical research subjects. An enormous amount of effort has been devoted to understanding shear yielding, crazing, cracking, and other micromechanical deformations in polymers.[2]

Irreversible micromechanical deformations have mainly been studied to understand and improve the mechanical properties of materials.[2–4] However, they can also be used for the processing of specialty materials. Crazing and microcracking phenomena can produce porous materials if they are properly controlled.[5–10] Currently, porous films are often produced by multiaxial stretching. Voids develop around inorganic particles embedded in a polyolefin matrix during stretching.[11–14]

In our previous study,[15] we explored a novel processing technique for making porous films by stretching incompatible polyolefin binary blends with a nearly 50/50 composition. Various porous structures were reported in the study.[15] The 50/50 blends have relatively large interfacial regions that can trigger pore development. The use of different polyolefins makes available a wide range of interfacial strengths,[16] which facilitates control over the stress concentration and pore development in the interfacial region.

Discrete nanopores are found in binary blends of metallocene polyolefins with a relatively high stress-to-break ratio.[15] This has led us to conclude that a relationship exists between discrete nanopore development and macroscopically stable tensile deformation without premature brittle failure. Thus, understanding the underlying mechanisms of discrete nanopore development will be useful for improving the efficiency and reliability of processing these unique porous polyolefin films.

For the purpose of this study, the initiation and growth of the discrete nanopores in the binary blends and layered films of polyolefins have been investigated in detail. Layered films do not have a local stress concentration caused by the curvature of the interface, so they offer an interesting comparison with blend systems. The binary systems used in this study have two semicrystalline polyolefins: polyethylene (PE) copolymers and polypropylenes (PPs). Semicrystalline polymers have complicated mechanical properties that are generally more difficult to understand and

Correspondence to: J. Lee, Department of Nano Science and Engineering, Sejong University, Kwang-Jin-Gu, Gun-Ja-Dong 98, Seoul, Korea (jlee@sejong.ac.kr).
Contract grant sponsor: ExxonMobil Co.

predict than those of amorphous polymers.[2,17,18] Thus, this study will also assist with the continuing effort to reveal how micromechanical deformations are initiated and developed in polyolefins,[19] particularly in 50/50 blends and layered films.

EXPERIMENTAL

Materials

PE copolymers and PPs were provided by ExxonMobil. The metallocene PE copolymers, Exact 4033 (PE-m1) and Exact 0201 (PE-m2), contain butene (11.4 mol %) and octene (4.6 mol%) comonomers, respectively.[20] The molecular weights of PE-m1 and PE-m2 are 118 and 78 kg/mol, and their melting points are 63 and 96°C, respectively. However, they have the same polydispersity of 2.1. The two PPs, Achieve PP3825 (PP-m) and Escorene PP4062 (PP-z), have weight-average molecular weights of 27 and 48 kg/mol and polydispersities of 2.0 and 2.4, respectively. The physical properties are described in detail elsewhere.[15] All the polymers were in a pelleted form and were used after being dried *in vacuo* at room temperature for 5 days.

Preparation of the films

The polymer pellets were mechanically mixed in a bottle for 2 min and melt-blended in a Haake Rheomix 600 at 190°C and 50 rpm (maximum shear rate = 65 s^{-1}). After 5 min of blending, the polymer melt was quenched in liquid nitrogen and vacuum-dried for 3 days. Films about 100 μm thick (stainless spacer = 277 $\pm$ 5 μm) were prepared from the blends via hot pressing at 190°C for 5 min (1 metric ton). The same hot pressing was used to prepare layered films with three different spacers (277 $\pm$ 5, 659 $\pm$ 9, and 1941 $\pm$ 10 μm) from already prepared films of each component polymer. The films were slowly cooled to room temperature (for ca. 30 min) and characterized after 3 days of physical aging at room temperature.

Characterization

An MTS MicroBionix mechanical tester with a 4-N load cell (10-mm span) was used to test rectangular specimens of the blends and layered films under ambient conditions. The displacement rate was controlled at 8 mm/min. For tensile tests, five rectangular specimens 8 mm wide and 18 mm long were used. For tear tests, four specimens 5 mm wide and 40 mm long were used. Because of the low modulus of the PE layers, the tear angle was approximately 160–180°. The specimen's dimensions were measured with an NSK Digitrix II micrometer (resolution = $\pm$1 μm). The displacement was calibrated with digital images of the specimens taken during stretching.

TABLE I
Tensile Properties of the Polymers

Polymer	Composition	Modulus (MPa)	Strain at break
PP-m		800 ($\pm$76)	0.3 ($\pm$0.2)
PP-z		1030 ($\pm$199)	0.2 ($\pm$0.1)
PE-ml		11 ($\pm$3)	7.5 ($\pm$0.6)
PE-m2		42 ($\pm$2)	8.8 ($\pm$0.6)
PP-m/PE-ml	60/40	456 ($\pm$22)	0.7 ($\pm$0.1)
	50/50	315 ($\pm$22)	6.4 ($\pm$1.0)
	40/60	297 ($\pm$44)	7.3 ($\pm$0.3)
	30/70	144 ($\pm$12)	8.1 ($\pm$0.6)
PP-z/PE-ml	60/40	419 ($\pm$55)	0.8 ($\pm$0.2)
	50/50	362 ($\pm$44)	0.5 ($\pm$0.1)
	40/60	158 ($\pm$34)	6.5 ($\pm$0.6)
	30/70	75 ($\pm$3)	6.4 ($\pm$1.3)
PP-m/PE-m2	60/40	479 ($\pm$66)	0.2 ($\pm$0.1)
	50/50	351 ($\pm$44)	0.8 ($\pm$0.5)
	40/60	317 ($\pm$14)	0.6 ($\pm$0.2)
	30/70	146 ($\pm$20)	10.3 ($\pm$0.3)

Values in parentheses are standard deviations.

For transmission electron microscopy (TEM), polyolefin films embedded in an epoxy resin (Tra-Con BA-2115 (Bedford, MA); cured for 24 h at room temperature) were microtomed at −120°C with a glass knife and then stained with RuO_4 for 6–24 h.[21–25] The stained films were then microtomed with a Microstar diamond knife to produce thin sections 70–80 nm thick. A TEM investigation was performed with a JEOL 1210 electron microscope at an accelerating voltage of 120 kV.

Scanning electron microscopy (SEM) was performed on Pt–Pd-coated (ca. 5 nm) specimens with a Hitachi S-800 field-emission-gun microscope at 3–5 kV. A Bruker AXS microdiffractometer with a 2.2-kW sealed Cu X-ray source and a Hi-Star two-dimensional (2D) area detector was used for a wide-angle X-ray scattering (WAXS) pattern study.[26]

RESULTS

Tensile tests of the blend films

The macroscopic tensile behavior of the binary polyolefin blends was has previously been reported in detail[15] and is summarized in Table I. As the content of PE increases, the modulus of the blends decreases, and the strain to break increases. Among the three blend systems with a 50/50 composition, PP-m/PE-m1 has the highest strain to break. In the PP-m/PE-m1 blends, brittle deformations, intrinsic to PP-m, are depressed by certain mechanisms, and this results in a high strain to break. Discrete nanopores, which appear to be related to the depression mechanism, were frequently found in the TEM investigation. Brittle-to-ductile transitions of the strain to break with an increase in the PE content occur at different compositions, depending on the binary system. A previous study[15] has shown that the transition does not fully

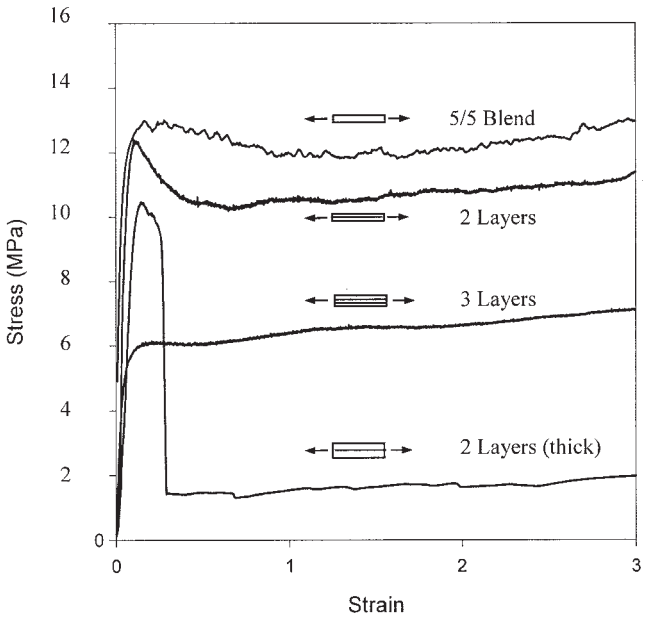

Figure 1 Stress–strain curves of tensile tests of PP-m/PE-1 blend and layered films. The average layer thickness values were 50 ± 4 μm for two layers (PP-m/PE-m1), 39 ± 3 μm for three layers (PE-m1/PP-m/PE-m1), and 510 ± 34 μm for two layers (PP-m/PE-m1; thick).

reflect the phase inversion[27] of blend morphology, suggesting the existence of other influences. (The detailed characterization results of the morphologies and mechanical properties of the blends can be found in ref. 15.)

Tensile tests of the layered films

The tensile stretching of layered films can provide a useful comparison for improving our understanding of the tensile behavior of 50/50 blends. The morphology of 50/50 blends varies widely and complicates the comparison of different systems. In contrast, the morphology of layered films is determined by processing and does not depend on the interfacial energies and viscosities of the component polymers. Furthermore, the interface of layered films is aligned along the tensile direction, and so no strong stress concentration effect exists near the interface.[28] After considerable shear yielding, interfaces in 50/50 blends generally align along the tensile direction,[15] and this results in 50/50 blends behaving similarly to films of many thin layers.

The typical tensile stress–strain curves of a 50/50 blend and layered films are provided in Figure 1. Two-layer films of two thicknesses were tested; the first film was considered thin with a thickness of 50 μm, and the second film was considered thick with an order of magnitude increase in thickness to 510 μm. The stress–strain curves of the two films were characterized by a sudden drop in stress after yielding, this being particularly distinct in the thicker films. While we tested the thick two-layer films, we noticed that the drop in stress resulted from the complete failure of PP layers. After the failure, PE layers stretched continually. The PP layer of the thin two-layer films did not fail abruptly after shear yielding (ca. 10–60% strain). Instead, it failed continuously and delaminated with the elongation of the PE layer.

The distinct drop in stress found in the stretching of the two-layer films was not observed in the tests of the thin three-layer films. Figure 1 shows that their stress–strain curves are similar to those of 50/50 blends. Differences between the two curves of the three-layer and 50/50 blend films exist in the absolute values of the modulus and yield stress. The differences are natural results and are attributed to the lower PP content in the three-layer films (ca. 33%). In the three-layer film, the failure of a PP layer cannot easily be observed because the layer exists between two PE layers. As the thickness of layers decreases and the number of layers increases, the tensile behavior of a layered film becomes similar to that of a 50/50 blend (Fig. 1).

Figure 2 shows the tensile behavior of three different pairs of polyolefins processed into two-layer films. Of the three films, the PP-m/PE-m1 film is the strongest (higher strain to failure); its PP layer simply delaminates after a drop in stress (10–60% strain), whereas the PP layers in PP-m/PE-m2 and PP-z/PE-m1 fail abruptly (<100% strain). The results of Figure 2 are consistent with the tensile test results of 50/50 blends (Table I), PP-m/PE-m1 showing the highest strain at break of other blends. Despite the

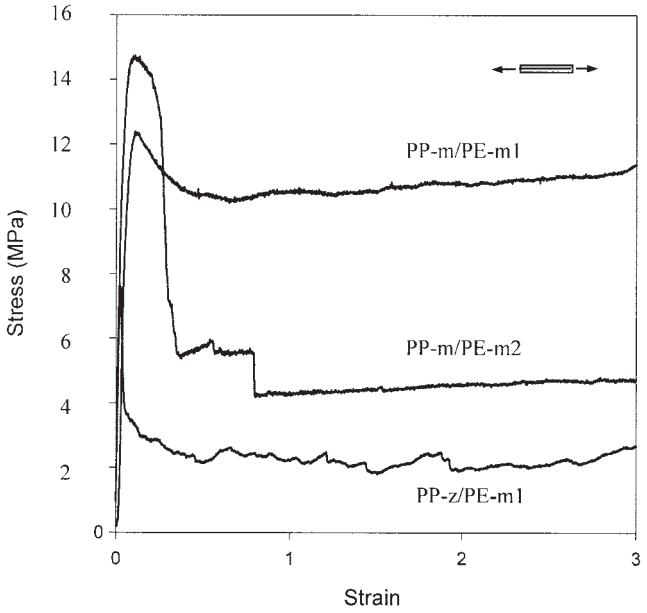

Figure 2 Stress–strain curves of tensile tests of two-layer films. The average layer thickness values were 50 ± 4 μm for PP-m/PE-m1, 55 ± 8 μm for PP-z/PE-m1, and 38 ± 7 μm for PP-m/PE-m2.

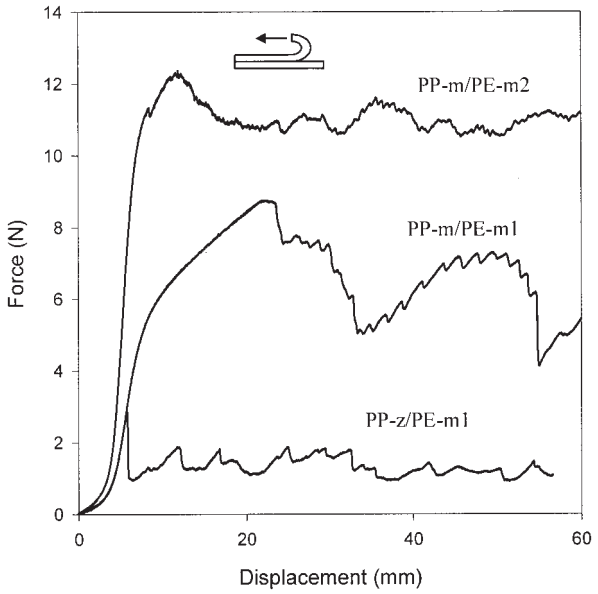

Figure 3 Force–displacement curves of the tear tests of two-layer films. The average layer thickness values were 510 ± 34 μm for PP-m/PE-m1, 414 ± 113 μm for PP-z/PE-m1, and 444 ± 81 μm for PP-m/PE-m2.

differences in the microstructures, the PP-m/PE-m1 metallocene pair has a higher strain to break in both 50/50 blends and layered films.

Tear tests of the layered films

The differences found in the tensile tests may be attributed to differences in the interfacial strength because macroscopic failure can be initiated by interfacial failure. The interfacial strength can be qualitatively assessed by tear tests. The interfacial strength measured in mode I failure[1,2] is an intrinsic material property that determines interfacial failure in blends and layered films with their morphological variables.

Typical force–displacement curves of the tear tests are given in Figure 3. These curves show rather unstable (stick–slip) crack propagation.[2,28] After an region with an initial increase (ca. 0–10-mm displacement), the tear force reaches a steady state. The stability of this crack propagation is determined by the competition between the energy-releasing rate and the material's resistance to crack propagation.[28] Despite unstable propagation, a qualitative comparison between different films is possible because uniform specimen and testing geometries were used. Tear tests were repeated with at least four specimens. No overlap between the tear-force curves of different blends was observed in their steady-state regimes. In other words, the differences in the steady-state tear forces were larger than their error.

Because PP-m/PE-m1 has the highest strain at break in the tensile tests of 50/50 blends (Table I), it might be expected to have the highest interfacial strength. However, Figure 3 shows that the interfacial strength of PP-m/PE-m1 is no better than that of PP-m/PE-m2. Consequently, the interfacial strength may play a role in stabilizing the stretching of the PP layer (phase) in tension, but it is not the only determining factor.

The results in Figure 3 are consistent with previous studies on the weld strength of polyolefin blends.[29–31] In previous studies,[29–31] it was found that noncrystallizable chains in Ziegler–Natta polyolefins could weaken the interface because of the absence of an interfacial anchoring mechanism.[29–31] In this study, PP-z/PE-m1 could have a similar weakened interface, although the effect is expected to be less distinct because of the relatively low crystallinity of PE-m1. Indeed, the relatively low interfacial strength of PP-z/PE-m1 is distinct in Figure 3.

Fractography

Fractography investigation with SEM is a convenient way of tracking the fracture process at interfaces.[2] PP and PE fracture surfaces produced in tear and tensile tests (delaminated surfaces) were found to be significantly different. The PP delaminated surfaces usually had more distinct features than the PE surfaces. Furthermore, differences among the different systems were more noticeable in the PP surfaces. (This might be due to the relatively high crystallinity of PP.) Therefore, the PP delaminated surfaces were used for our analysis.

Figure 4 provides SEM micrographs of PP delaminated surfaces. The evidence of spherulite structures[32] is distinct in PP-m/PE-m1 and PP-m/PE-m2 but not in PP-z/PP-m1. The tearing of microfibrils[2] seems to occur in PP-z/PE-m1, and this results in the features of Figure 4(c). The existence of the features is consistent with the argument that PP-z/PE-m1 has accumulated amorphous chains in its interfacial region.[29–31]

The area under the curves in Figure 3 shows that energy absorption through the tearing of microfibrils during interfacial failure is relatively small. The low interfacial (adhesive) failure energy will prevent cohesive failure from occurring in the PE phase of PP-z/PE-m1. If it occurs, although this is an unrealistic scenario, the cohesive failure itself could produce fracture surface features similar to those shown in Figure 4(c).

Shear yielding

The premature brittle failure of PP phases can be observed in the stress–strain curves of two-layer PP-m/PE-m1 (Fig. 1). When the failure is suppressed in thin three-layer films or 50/50 blends (Fig. 1), shear yielding continues to develop and produce significant anisotropy in their molecular structures. The anisotropy can simply be checked by 2D WAXS patterns,[26] as shown in Figure 5. More significant anisotropy can be found in the three-layer system and the 50/50

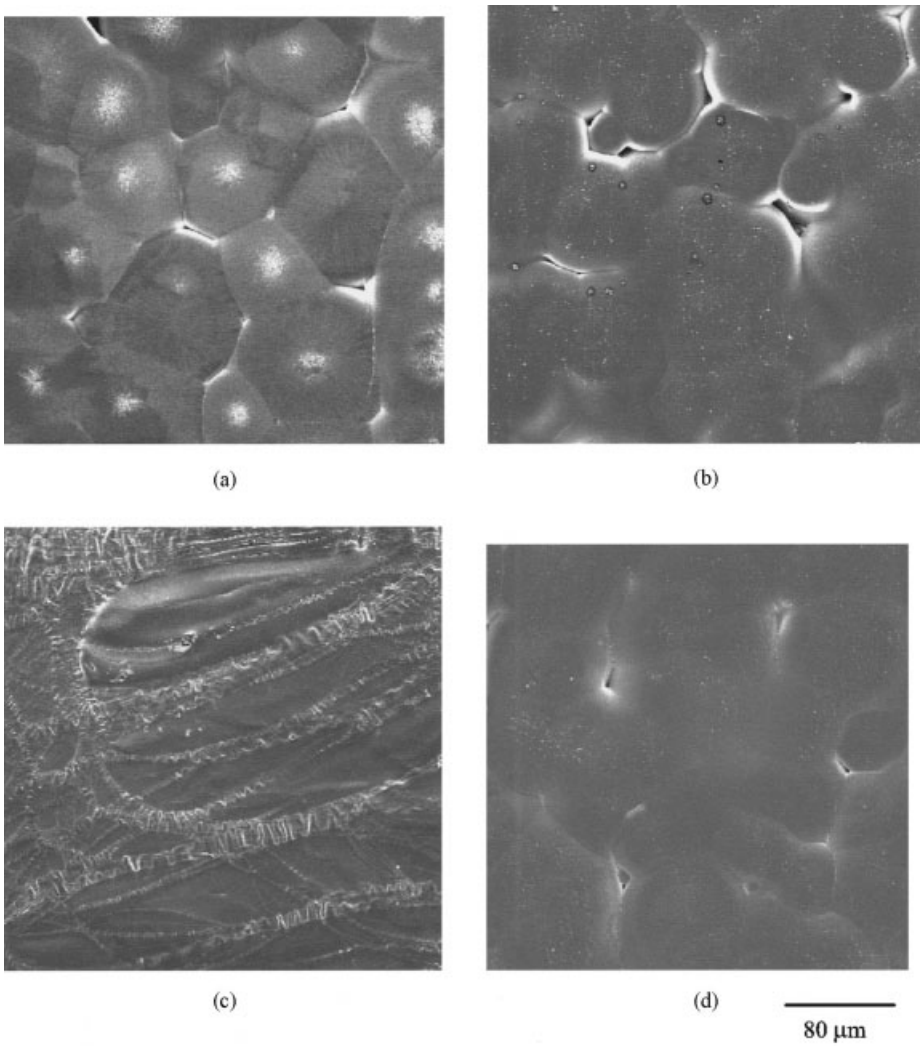

Figure 4 SEM micrographs of the delaminated surfaces of PP layers broken in the tear and tensile tests of two-layer films: (a) PP-m/PE-m1, tension; (a) PP-m/PE-m1, tear; (a) PP-z/PE-m1, tear; and (a) PP-m/PE-m2, tear. The fracture surface initially faced the PE layers.

blend than in the two-layer specimen. Because the crystallinity of PE is only 5%, it is difficult to exclude the diffraction contribution from PP crystals. Thus, the 2D WAXS patterns prove that significant shear yielding actually occurs in PP, particularly in the PP phases of the three-layer and 50/50 blend systems.

Tem microscopy: layered films

As previously shown, the existence of ductile PE (or its micromechanical deformations) has the effect of suppressing brittle failure and promoting shear yielding in its neighbor PP phase. A TEM investigation of subcritical deformations in the PP phase confirms those effects and is shown in Figures 6–9. The primary question here is how to stabilize brittle micromechanical deformations in the PP phase.

The brittle fracture of PP polymers generally occurs within their stress-whitened regions, which contain crazes (or crazelike structures),[17,33,34] voids, or microcracks. Among the possible sources of stress whitening, crazelike structures are predominantly observed. Figure 6 provides a typical TEM micrograph of multiple crazelike-structure bands that have developed perpendicularly to the direction of the far-field stress.[2] They can easily grow into critical cracks and trigger brittle failure.

Crazelike-structure development in two-layer films (Fig. 7) is different from what pure PP shows in Figure 6, although the PP layer is as thick as 510 μm. There are two distinct types of crazelike structures, as shown in Figure 7. One is the same linear crazelike-structure band shown in Figure 6 [Fig. 7(a)]. These bands usually exist perpendicular to the direction of the far-field stress, and their length spans from several hundreds of nanometers to micrometers. The other type of crazelike structure is irregular rather than linear. Figure 7(b) shows irregular crazelike structures, which are generally distributed along the fracture surface. The irregular crazelike structures are composed of discrete or agglomerated pores (dark spots of ca.

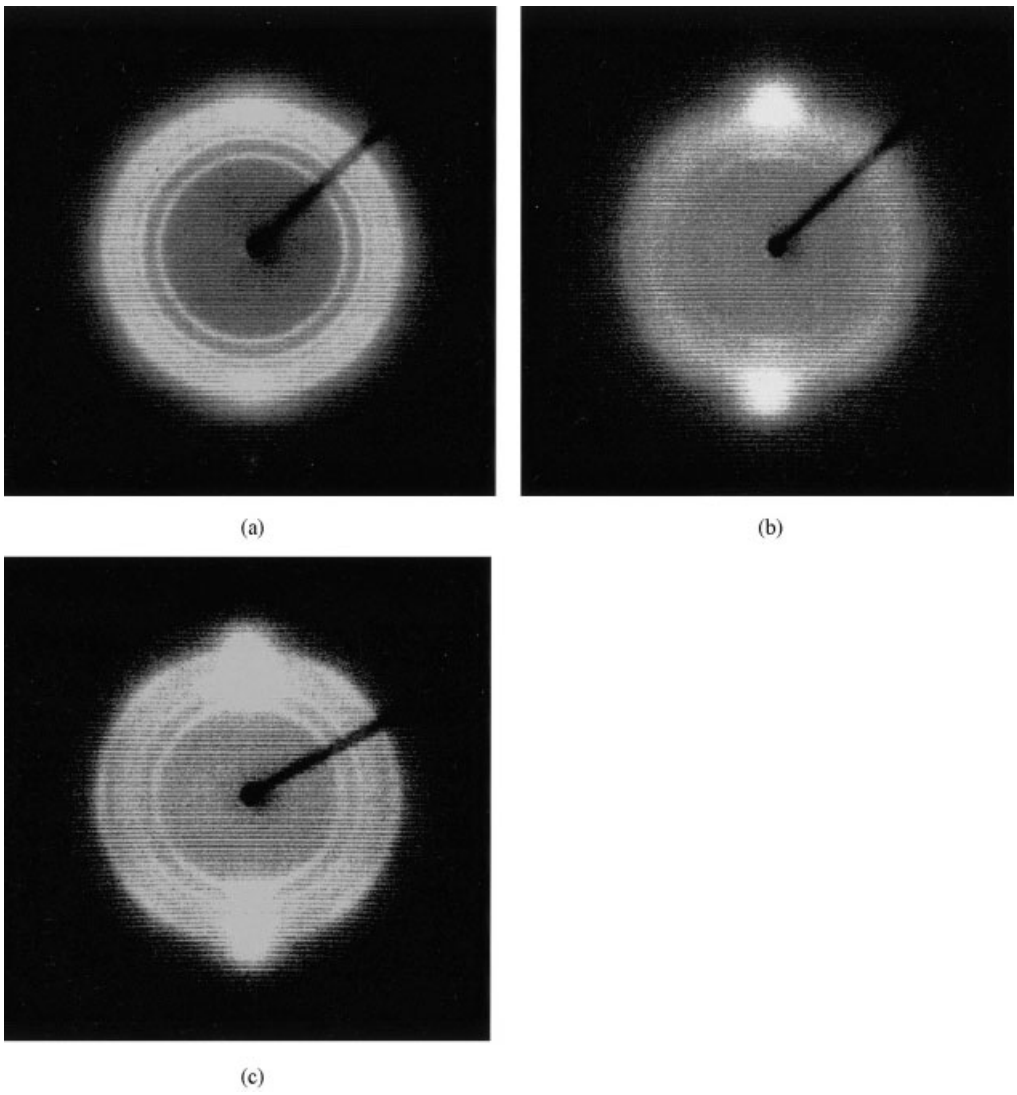

Figure 5 2D WAXS patterns of PP-m/PE-m1 films broken in tensile tests: (a) two layers (PP-m/PE-m1; layer thickness = 50 ± 4 μm), (b) three layers (PE-m1/PP-m/PE-m1; layer thickness = 39 ± 3 μm), and (c) a 50/50 blend.

10–50 nm), which seem to result from the disruption of crazelike structures. The fracture surface originally faced a PE layer before the tensile tests. The existence of the PE layer is related to the formation of this irregular crazelike structure. Because the same irregular crazelike-structure pores were not found in the freestanding PP-m film (Fig. 6), they are not a direct result of the plane stress condition. It can be conjectured from the size and shape of the crazelike structures that the crazelike-structure bands in Figure 7(a) are less stable upon stretching than those in Figure 7(b).

The similarly disrupted nanopores shown in Figure 7(b) can be found in thin two-layer films [Fig. 8(a)] and blends (Fig. 9). Thin films (layer thickness = ca. 50 μm) of both metallocene and Ziegler–Natta pairs (PP-z/PE-m1) show nanopores (Fig. 8). Like the nanopores in Figure 7(b), the majority of the nanopores exist near the fracture surface of PP; this indicates the effect of the PE layer across the interface. Some nanopores align linearly, as shown in Figure 8(a). Thus, the disrupted nanopores apparently result from the initial crazelike-structure band structures. The same nanopores shown in Figure 8(a) were occasionally observed in thin two-layer films of PP-m/PE-m1. However, the majority of the thin sections did not contain a significant number of nanopores, as shown in Figure 8(b).

TEM microscopy: blend films

Under tension, 50/50 blend systems inherently have higher local stress concentrations than layered films. (Even in layered films, a weak stress concentration is inevitably generated at the interfacial regions because of the difference in the moduli.[28]) Because the local stress concentration will facilitate the initiation of crazelike structures, crazelike structures should be more frequently observed in 50/50 blend systems. Indeed, that was the case in this study (Figs. 8 and 9).

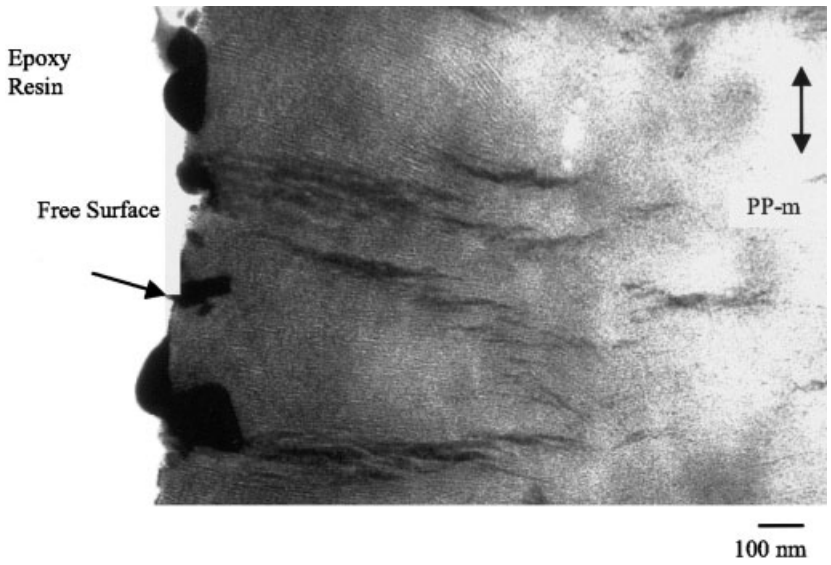

Figure 6 TEM micrograph of a PP-m film (70 μm thick) broken under uniaxial tension. The arrow indicates the direction of the far-field stress. Crazes developed perpendicularly to the direction of the far-field stress. The dark spots on the film surface were OsO_4-stained impurities.

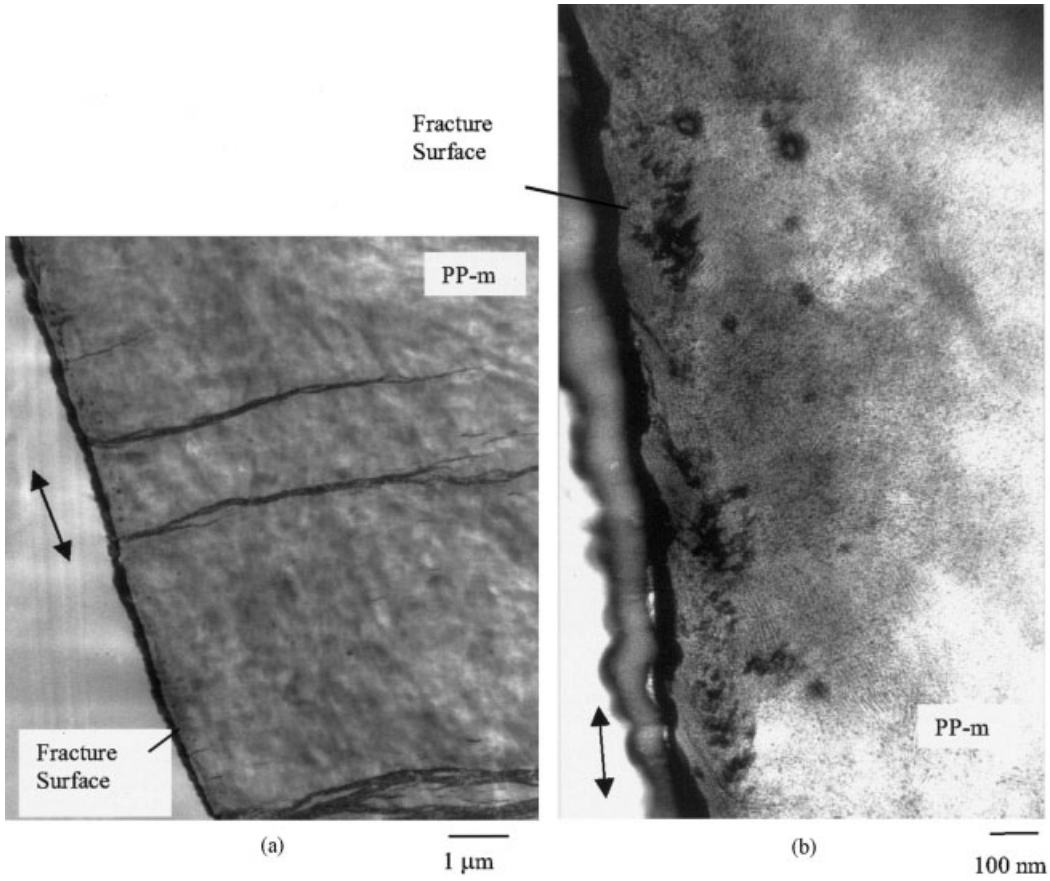

Figure 7 TEM micrographs of PP layers in two-layer films of PP-m/PE-m1 (layer thickness = 510 $\pm$ 34 μm) broken under uniaxial tension: (a) low and (b) high magnification. The arrows indicate the direction of the far-field stress.

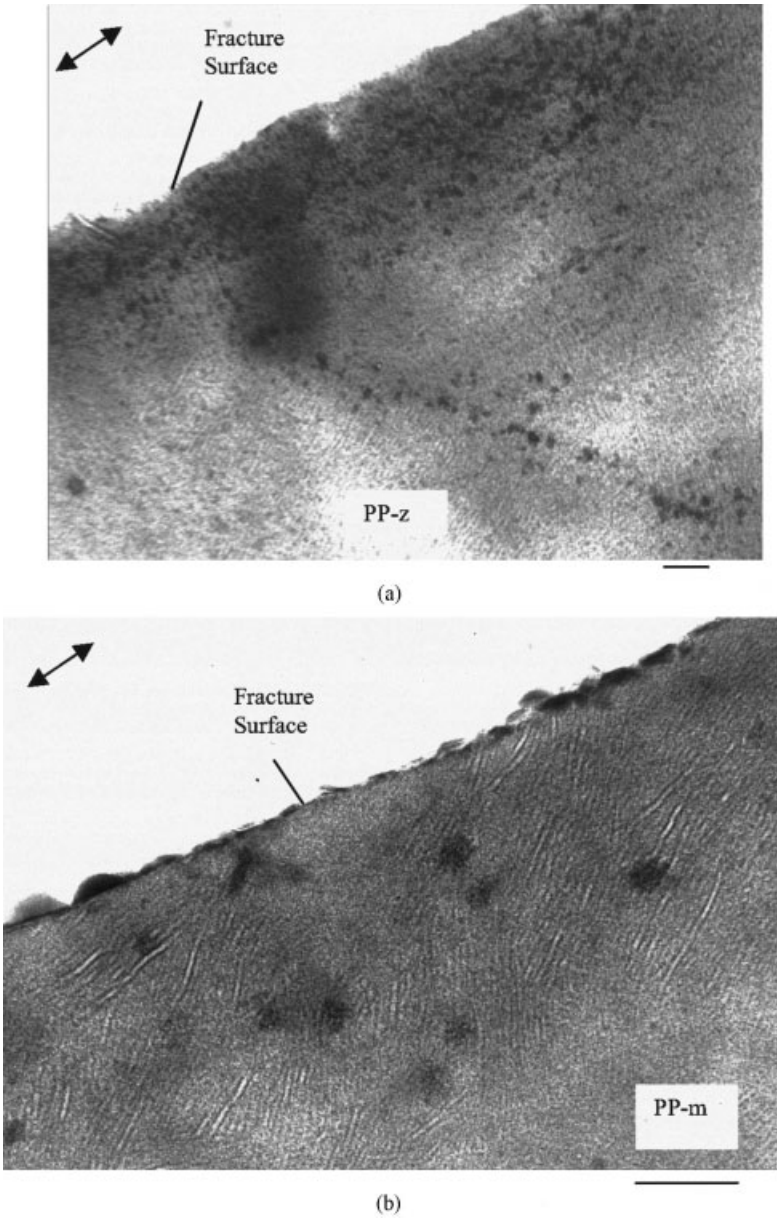

Figure 8 TEM micrographs of PP layers in layered films broken under uniaxial tension: (a) two-layer film of PP-z/PE-m1 (layer thickness = 55 ± 8 μm) and (b) two-layer film of PP-m/PE-m1 (layer thickness = 50 ± 4 μm). The scale bar is 100 nm. The arrows indicate the direction of the far-field stress.

Figure 9(a) shows the initial development of crazelike structures in the 50/50 blends of PP-m/PE-m1 (strain = 0.4). The nanopores are nearly lined up as band structures perpendicular to the direction of the far-field stress. Upon further tension, the crazelike structures become disrupted into discrete nanopores, as shown in Figure 9(b). In addition to discrete nanopores, well-developed crazelike-structure bands can also be found in broken specimens [Fig. 9(c)]. They exist in the stress-whitening regions of PP-m/PE-m2 and PP-z/PE-m1 too. As the band structure grows, it spans the whole PP phase between two PE phases, inducing crack initiation. Figure 9(d) shows fully grown band structures and the initiation of subsequent microcracking. Well-developed crazelike-structure bands and submicrometer cracks (not discrete nanopores) were frequently observed in PP-m/PE-m2 and PP-z/PE-m1. The contraction of the PP region around the submicrometer crack in Figure 9(d) indicates that crazelike-structure development induces micronecking.[35] If this happens, a stronger interface could partially suppress the development of crazelike structures into critical cracks.

DISCUSSION

The series of events occurring in the tension of systems of 50/50 blends and layered films, particularly in their PP phases, can be classified into two cases: brittle

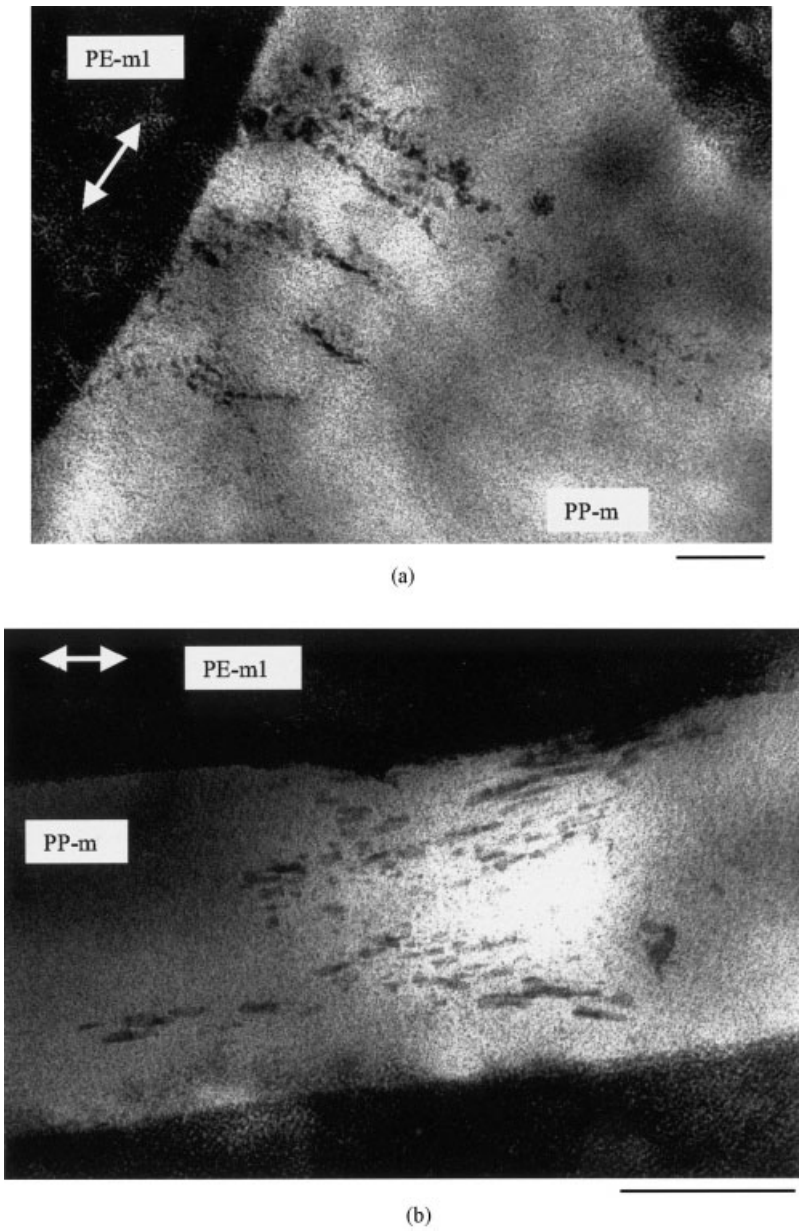

Figure 9 TEM micrographs of crazes in polyolefin blend films under uniaxial tension: (a) PP-m/PE-m1 (50/50; strain = 0.4), (b,c) PP-m/PE-m1 (50/50; broken), and (d) PP-z/PE-m1 (50/50; broken). The scale bar is 200 nm. The arrows indicate the direction of the far-field stress.

and ductile. Both PP-z/PE-m1 and PP-m/PE-m2 systems show relatively brittle behavior, whereas PP-m/PE-m1 shows quite different ductile behavior. In layered-film systems, as the layer thickness decreases, more ductile behavior results. In the brittle cases, tensile stretching initiates crazelike structures, and they mostly develop into band structures, microcracks, and macroscopic cracks, resulting in premature failure. In the ductile cases, the initiation of crazelike deformations is followed by stable shear yielding until macroscopic failure. Crazelike structures are disrupted into discrete nanopores during the stable-shear-yielding period.

The major difference between the two behaviors is whether the disruption mechanism of crazelike structures is active; this prevents the further growth of crazelike structures into microcracks and macrocracks. Discrete nanopores formed by this mechanism were observed in systems with a wide range of internal morphologies, from layered films to 50/50 blend systems, although their number density was higher in blend systems. In most cases, nanopores were found near the interfacial regions between PP and PE. They seem to originate from the interfaces.

Crazing generally depends on two factors: local stress conditions and material characteristics. Both factors need to be considered to understand the disruption mechanism of crazelike structures. Generally, the triaxial stress component is responsible for the development of crazelike structures, whereas the deviatory

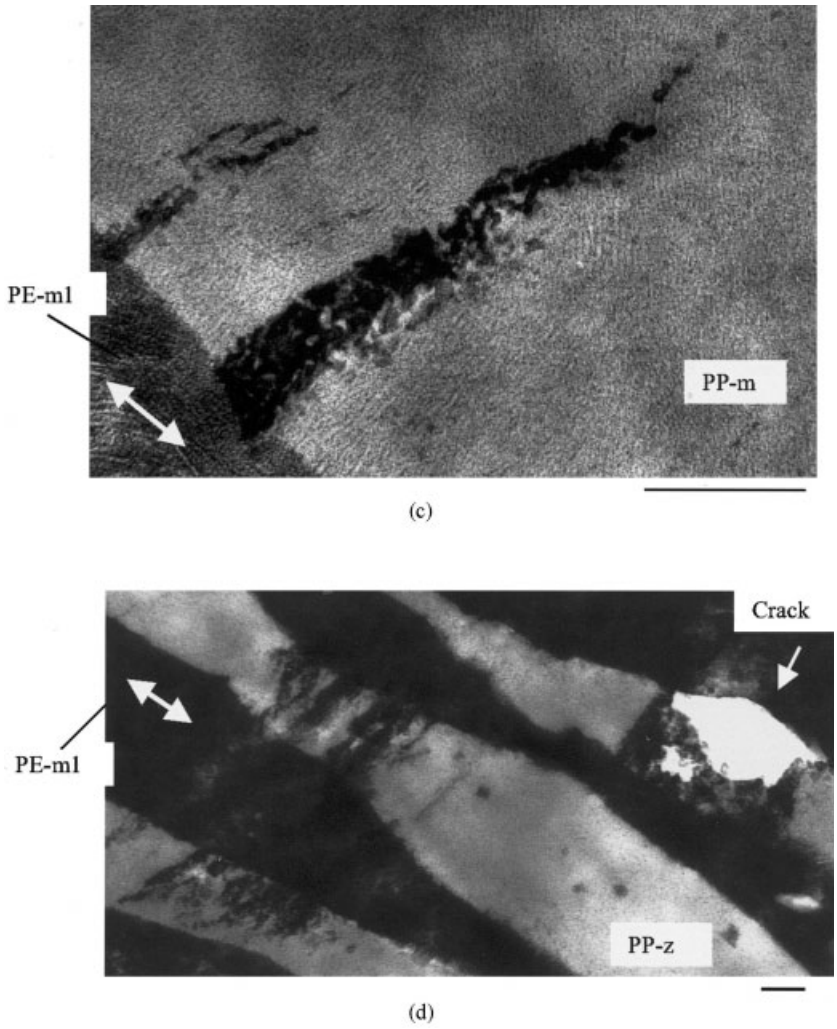

Figure 9 (*Continued*)

stress component is responsible for shear yielding. Therefore, for crazelike-structure disruption and shear yielding to prevail in PP phases, local stress conditions should change after the initiation of crazelike structures.

Shear yielding in a PE phase can increase the local deviatory stress component[28] in the adjacent PP phase, and this will facilitate the initiation of shear yielding. Our experimental observations indicate that this enhanced shear yielding plays an important role in disrupting crazelike structures. Supporting experimental results on the influence of an adjacent phase have been reported elsewhere.[35–42] For example, the study of microlayered films[36] has shown that shear yielding in one phase can induce shear yielding in the adjacent phase. It has also been observed[36] that the failure of layered films becomes more ductile as the layer thickness becomes smaller. Furthermore, dilatational deformations such as crazing can partially increase the local deviatory stress, and this results in the facilitation of shear yielding. Thus, shear yielding might easily follow the initiation of crazelike structures.

Shear yielding may not be the only source triggering the disruption process. At the interface between PP and PE, PP chains can develop into a crystal structure different from bulk crystalline structures, which can then induce different micromechanical deformations. The possibility of induced crystallization at an interface has been previously reported.[43,44]

Differences in material characteristics should be considered to understand the outstanding mechanical behavior of PP-m/PE-m1 systems. The material parameters found to be related to the mechanical behavior are (1) the intrinsic mechanical properties of PE, such as the yield stress; (2) the internal morphology, such as spherulitic structures; and (3) the interfacial strength between PP and PE. They are all important factors contributing to the formation of discrete nanopores in a PP phase. However, none of the properties alone can explicitly explain the mechanical behaviors of PP-m/PE-m1 systems.

PE-m1 has the lowest yield stress, and this yielding behavior may be related to the disruption mechanism of PP-m/PE-m1 systems. However, the same material

alone could not successfully induce the same disruption mechanism in PP-z/PE-m1 blends.

The internal morphology is a critical parameter determining local stress conditions in blends. Layered films and 50/50 blends have significantly different morphologies, but interestingly, similar disruption mechanisms are found in both systems. The comparison between layered films and blends reveals that morphology is an important factor but is not the only one determining the disruption mechanism. The interfacial strength is also shown to be important in Figure 3. In general, a strong interface and a lower yield stress seem to be favorable for the formation of discrete nanopores. Because they usually develop near interfaces, increasing the interfacial area will increase the density of nanopores.

CONCLUSIONS

The development of nanopores under tension has been examined with blends and layered films of metallocene and Ziegler–Natta polyolefins. Discrete nanopores have been found in both the blends and layered films, typically near their interfacial regions. The interactions between the PE copolymers and PPs play a significant role in the development of the nanopores. The existence of an adjacent ductile PE copolymer or its micromechanical deformations suppresses craze (crazelike-structure) growth and induces shear yielding in PP. In this process, crazelike structures of initial growth stages become disrupted into discrete nanopores. Otherwise, they would develop into mature craze bands and initiate brittle failure. These results agree with the macroscopic mechanical performances of the blends and layered films, which are significantly influenced by the existence of the disruption mechanism.

The authors are indebted to Pat Brant for insightful comments and to David Bell for technical training for transmission electron microscopy.

References

1. Gere, J. M.; Timoshenko, S. P. Mechanics of Materials; PWS: Boston, 1990.
2. Kinloch, A. J.; Young, R. J. Fracture Behavior of Polymers; Elsevier: Amsterdam, 1985.
3. Bucknall, C. B. Toughened Plastics; Applied Science: London, 1977.
4. Lee, J.; Yee, A. F. Polymer 2001, 40, 589.
5. Druin, M. L.; Loft, J. T.; Plovan, S. G. U.S. Pat. 3,801,404 (1974).
6. Kamada, K.; Minami, S.; Toshida, K. U.S. Pat. 4,055,696 (1977).
7. Chen, R. T.; Saw, C. K.; Jamieson, M. G.; Aversa, T. R.; Callahan, R. W. J Appl Polym Sci 1994, 53, 471.
8. Kim, J.-J.; Jang, T.-S.; Kwon, Y.-D.; Kim, U. Y.; Kim, S. S. J Membr Sci 1994, 93, 209.
9. Garg, D. H.; Lenk, W.; Berwald, S.; Lunkwitz, K.; Simon, F.; Eichhorn, K.-J. J Appl Polym Sci 1996, 60, 2087.
10. Chandavasu, C.; Xanthos, M.; Sirkar, K. K.; Gogos, C. G. Annu Tech Conf Proc 2000, 2, 2458.
11. Nago, S.; Mizutani, Y. J Appl Polym Sci 1996, 61, 31.
12. Nago, S.; Mizutani, Y. J Appl Polym Sci 1998, 68, 1543.
13. Mizutani, Y.; Nago, S. J Appl Polym Sci 1999, 72, 1489.
14. Colvin, R. Mod Plast 2000, 24.
15. Lee, J.; Macosko, C. W.; Bates, F. S. J Appl Polym Sci 2004, 91, 3642.
16. Weimann, P. A.; Jones, T. D.; Hillmayer, M. A.; Bates, F. S.; Londono, J. D.; Melnichenko, Y.; Wignall, G. D.; Almdal, K. Macromolecules 1997, 30, 3650.
17. Starke, J. U.; Michler, G. H.; Grellmann, W.; Seidler, S.; Gahleitner, M.; Fiebig, J.; Nezbedova, E. Polymer 1998, 39, 75.
18. Michler, G. H. Polym Adv Technol 1998, 9, 812.
19. Karger-Kocsis, J. Macromol Symp 1999, 143, 185.
20. Yamaguchi, M.; Miyata, H. Macromolecules 1999, 32, 5911.
21. Trent, J. S.; Scheinbeim, J. I.; Couchman, P. R. Macromolecules 1983, 16, 589.
22. Montenzinos, D.; Wells, B. G.; Burns, J. L. J Polym Sci Polym Lett Ed 1985, 23, 421.
23. Sano, H.; Usami, T.; Nakagawa, H. Polymer 1986, 27, 1497.
24. Brown, G. M.; Butler, J. H. Polymer 1997, 38, 3937.
25. Lednicky, F.; Coufalova, E.; Hromadkova, J.; Delong, A.; Kolarik, V. Polymer 2000, 41, 4909.
26. Campbell, D.; White, J. R. Polymer Characterization: Physical Techniques; Chapman & Hall: London, 1989; p 154.
27. Willemse, R. C.; Speijer, A.; Langeraar, A. E.; Posthuma de Boer, A. Polymer 1999, 40, 6645.
28. Williams, J. G. Fracture Mechanics of Polymers; Ellis Horwood: Hemel Hempstead, England, 1984.
29. Chaffin, K. A. Ph.D. Thesis, University of Minnesota, 1999.
30. Chaffin, K. A.; Bates, F. S.; Brant, P.; Brown, G. J Polym Sci Part B: Polym Phys 2000, 38, 108.
31. Chaffin, K. A.; Knutsen, J. S.; Brant, P.; Bates, F. S. Science 2000, 288, 2187.
32. Wignall, G. D.; Alamo, R. G.; Londono, J. D.; Mandelkern, L.; Kim, M. H.; Lin, J. S.; Brown, G. M. Macromolecules 2000, 33, 551.
33. Bretz, P. E.; Hertzberg, R. W.; Manson, J. A. Polymer 1981, 22, 1272.
34. Michler, G. H. Makromol Chem Macromol Symp 1991, 41, 39.
35. Lin, C. H.; Yang, A. C.-M. J Mater Sci 2000, 35, 4231.
36. Ma, M.; Vijayan, K.; Hiltner, A.; Baer, E.; Im, J. J Mater Sci 1990, 25, 2039.
37. Pan, S. J.; Im, J.; Hill, M. J.; Keller, A.; Hiltner, A.; Baer, E. J Polym Sci Part B: Polym Phys 1990, 28, 1105.
38. Shin, E.; Hiltner, A.; Baer, E. J Appl Polym Sci 1993, 47, 269.
39. Sung, K.; Haderski, D.; Hilter, A.; Baer, E. J Appl Polym Sci 1994, 52, 147.
40. Haderski, D.; Sung, K.; Im, J.; Hiltner, A.; Baer, E. J Appl Polym Sci 1994, 52, 121.
41. Sung, K.; Haderski, D.; Hiltner, A.; Baer, E. J Appl Polym Sci 1994, 52, 135.
42. Qureshi, N. Z.; Rogunova, M.; Stepanov, E. V.; Capaccio, G.; Hiltner, A.; Baer, E. Macromolecules 2001, 34, 3007.
43. Manaure, A. C.; Muller, A. J. Macromol Chem Phys 2000, 201, 958.
44. Laurens, C.; Ober, R.; Creton, C.; Leger, L. Macromolecules 2001, 34, 2932.